

# Differentiation of BIRADS-4 small breast lesions via Multimodal Ultrasound Tomography

G. Zografos · P. Liakou · D. Koulocheri · I. Liovarou ·  
M. Sofras · S. Hadjiagapis · M. Orme · V. Marmarelis

Received: 14 April 2014 / Revised: 20 August 2014 / Accepted: 26 August 2014 / Published online: 14 September 2014  
© European Society of Radiology 2014

## Abstract

**Purpose** To demonstrate the use of a new 3D diagnostic imaging technology, termed Multimodal Ultrasonic Tomography (MUT), for the detection of solid breast lesions <15 mm in maximum dimension.

**Methods and materials** 3D MUT imaging was performed on 71 volunteers presenting BIRADS-4 nodules, asymmetrical densities, and architectural distortions in X-ray mammograms, who subsequently underwent biopsy. MUT involved D tomographic imaging of the pendulant breast in a water bath using transmission ultrasound and constructed multimodal images

corresponding to refractivity and frequency-dependent attenuation (calibrated relative to water). The multimodal images were fused into composite images and a composite index (CI) was calculated and used for diagnostic purposes. The composite images were evaluated against results of histopathology on biopsy specimens.

**Results** Histopathology revealed 22 malignant and 49 benign lesions. The pixels of 22 malignant lesions exhibited high values in both refractivity and attenuation, resulting in CI values >1. In contrast, 99.9 % of benign lesions and normal tissue pixels exhibited lower values of at least one of the attributes measured, corresponding to CI values <1.

**Conclusions** MUT imaging appears to differentiate small malignant solid breast lesions as exhibiting CI values >1, while benign lesions or normal breast tissues exhibit CI values <1.

## Key Points

- MUT was able to detect all 22 biopsy-confirmed malignant lesions.
- MUT was able to differentiate the malignant from the benign lesions.
- Additional MUT detections outside the biopsy area must be evaluated prospectively.

G. Zografos · P. Liakou  
Breast Unit, University of Athens School of Medicine, Athens, Greece

G. Zografos  
e-mail: gzografo@med.uoa.gr

P. Liakou  
e-mail: liakoup@hotmail.com

D. Koulocheri  
Department of Radiology, Hippokration Hospital, Athens, Greece  
e-mail: dimitrakoul@gmail.com

I. Liovarou · M. Sofras · S. Hadjiagapis · M. Orme · V. Marmarelis  
Mastoscopia S.A., Athens, Greece

I. Liovarou  
e-mail: liovaroue@hotmail.com

M. Sofras  
e-mail: m.sofras@gmail.com

S. Hadjiagapis  
e-mail: s.d@mastoscopia.com

M. Orme  
e-mail: orme.melissa@gmail.com

V. Marmarelis (✉)  
Department of Biomedical Engineering, University of Southern California, DRB160, University Park, Los Angeles, CA 90089, USA  
e-mail: vzm@usc.edu

**Keywords** Breast cancer detection · Ultrasound tomography · Multimodal ultrasound · Lesion differentiation · 3D breast imaging

## Abbreviations

MUT	Multimodal Ultrasound Tomography
BIRADS	Breast Imaging Reporting and Data System
IDC	Invasive ductal carcinoma
DCIS	Ductal carcinoma in situ
CC	Craniocaudal
MLO	Mediolateral oblique

## Introduction

X-Ray mammography remains the “gold standard” for breast cancer screening despite its modest sensitivity (approximately 80 %) and specificity (approximately 85 %), especially for dense breasts (sensitivity of approximately 60 %) and lesions smaller than 1 cm [1–5]. This is due in part to the lack of cost-effective alternatives with higher sensitivity and specificity. Although MRI has been shown to have higher sensitivity than mammography, it exhibits low specificity and remains rather expensive and less accessible to the general population [6–8]. The use of echo-mode ultrasound (B-mode), either handheld or 3D automated, offers overall performance comparable to X-ray mammography for non-dense breasts, and constitutes a useful adjunct for cyst differentiation. Importantly, B-mode ultrasound, as an adjunct examination to mammography, appears to be more effective than X-ray mammography alone for dense breasts [9, 10]. The use of B-mode imaging for differentiation between benign and malignant lesions in the human breast has been explored using morphological features regarding lesion shape, size, and boundary [11–14]. Recent extensions of X-ray mammography in the form of tomosynthesis [15] and B-mode imaging in the form of 3D automated whole-breast ultrasound [16] appear to offer some marginal improvement in performance. The use of elastography as an adjunct to handheld B-mode imaging has shown initial promise in improving specificity [17, 18], but its sensitivity remains limited and its clinical use is confounded by practical issues.

In order to improve the sensitivity and specificity of breast cancer screening, over the last 14 years we have developed and tested a 3D diagnostic imaging technology, termed Multimodal Ultrasound Tomography (MUT). Relying on the longstanding empirical observation that malignant breast lesions exhibit micromechanical properties that are different from benign lesions or normal breast tissue, MUT achieves lesion differentiation on the basis of micro-mechanical tissue properties computed from tomographic images of acoustic refractivity and frequency-dependent attenuation [19–27]. The MUT imaging modality is distinctly different from conventional echo-mode ultrasound imaging (B-mode) because it constructs tomographic images in *transmission mode*, depicting the distribution of values of the acoustic attributes of refractivity and frequency-dependent attenuation at each tissue voxel rather than constructing morphological maps of acoustic reflection interfaces. The multiple MUT images (modes) are extracted from analysis of *waveform changes* in the received pulse after traversing the breast tissue (relative to water-through propagation) and not from analysis of the received pulse-echoes as in conventional B-mode imaging.

An early ultrasound tomography system for breast cancer detection was developed in the 1980s, but its clinical testing was inconclusive [28–30]. Another system with some capability for ultrasound tomography (distinct from MUT in its

data collection and analysis procedures) has been described in the literature, although no clinical results have yet been reported [31]. The first presentation of initial MUT clinical results was made at the 2011 European Congress of Radiology [23, 24], and MUT results from 25 volunteers with large BIRADS-5 lesions (>1 cm) were recently published as an initial demonstration of the efficacy of MUT [32]. This paper is a follow-up study on 71 female volunteers presenting mammographic BIRADS-4 nodules, asymmetries of density, and architectural distortions, who underwent MUT scanning prior to stereotactic biopsy. The biopsy-confirmed lesions offer the means for validation of the MUT results.

## Methods and materials

The clinical MUT prototype and its basic operation have been described in a recent publication [32]. To assist the reader, we summarize below the key operational features [19–24]. The MUT system performs 3D tomographic examinations of the pendulant breast in a fixed-coordinate system. The patient lies prone on a clinical bed with one breast inserted through a circular opening into a cylindrical imaging chamber containing precisely conditioned water bath. On one side of the imaging chamber, transducers transmit specially designed sequences of pulses that traverse the breast tissue and are received by transducers on the opposite side of the imaging plane. This procedure is repeated for multiple view-angles and elevations so that the whole breast parenchyma is examined. The in-plane pixel size is 0.25 mm×0.25 mm, and the separation between adjacent coronal images is set at 4 mm in this study (adjustable). The MUT examination takes approximately 10 minutes per breast, and the computation of all MUT images is completed in less than two minutes. All safety precautions are taken to eliminate electromechanical or hygienic risks for the patients.

For MUT image formation, waveform changes of the received pulses are analysed relative to their transmitted counterparts in order to extract the following acoustic attributes at each tissue voxel: refractivity (based on measurements of speed of sound in tissue relative to water) and frequency-dependent attenuation ranging from 1 to 5 MHz (2 and 4 MHz were used in this study). The values of these acoustic attributes are calibrated relative to water-through transmission (under precisely controlled conditions of water temperature, degasification, deionization, and filtering) to retain global numerical validity for comparative diagnosis across subjects and time. According to Stokes' law of acoustic attenuation that relates the frequency-dependent attenuation to the speed of sound through viscoelastic materials, these acoustic attributes quantify the micromechanical properties of compressibility and viscoelasticity of the cellular tissue structure.

For each coronal slice of the breast, multiple MUT images, corresponding to refractivity and frequency-dependent attenuation of each tissue voxel (or image pixel), were obtained. These two distinct component images were combined in product (using only their water-calibrated positive values) to form the *composite image* for each coronal slice based on the *values of the composite index* (CI) at each pixel. The 3D stack of coronal composite images (1–4 mm apart, depending on clinical requirements) allows complete screening of the entire breast volume in a 3D fixed-coordinate system, independent of human operator, yielding automatically calibrated measures of the micromechanical properties of the tissue/lesion voxels that are fused into the scalar CI value (calibrated to precisely controlled water-through reference).

In terms of data analysis, since there is some statistical variation in the measurements, the determination of a “diagnostic threshold value” is possible only in a statistical context, whereby the statistical significance level for characterizing a tissue voxel as malignant (when its CI exceeds some specified threshold value) can be determined by empirically computed statistical distributions of the measured attributes of non-malignant tissue voxels (serving as the Null Hypothesis). The composite MUT images serve the purpose of easily identifying the presence of possible lesions as having high CI values and can expedite diagnosis (when their reliability is confirmed). A colour-coding scheme is used for display in which deep blue corresponds to the lowest values and dark red to the highest values of CI, with the values in between following the gradations of the colour sequence in the visible spectrum (as indicated in a displayed colour bar).

Female volunteers were recruited from January 2011 to March 2013 at the Breast Unit of the First Propaedeutic Department of Surgery at the University of Athens, School of Medicine, in the Hippokration Hospital (“off-label” use for research purposes only). Female patients who were classified as BIRADS-4 based on mammogram findings and referred to biopsy as part of established clinical practice were given the option of being examined with the MUT system, provided that the maximum coronal diameter of their breast was less than 16 cm, their weight was less than 100 kg, and the mammographic finding was not very close to the pectoral muscle. None of the invited women refused to participate. For this particular study, the patient group included 71 female volunteers, average age 58.6 years (range 23–79), diagnosed by two independent radiologists, with BIRADS-4 nodules (<15 mm), density asymmetries, and architectural distortions in their mammograms. All patients were referred to stereotactic biopsy as part of standard clinical practice. Prior to biopsy, they underwent MUT imaging after signing the informed consent form approved by the Hospital Ethics Committee. There were no operational complications in any of the MUT images, and all volunteers attested to the total comfort of the imaging procedure. After the MUT examination, all patients proceeded

uneventfully with the stereotactic biopsy, which was performed on the digital prone table MammoTest Breast Biopsy System (Fischer Imaging Corporation). All lesions were successfully identified and subsequently retrieved under local anaesthesia using the Intact™ Breast Lesion Excision System (BLES) (Intact Medical Corporation). All specimens were examined by the same Breast Unit pathologists. The MUT results were evaluated by two independent radiologists on the basis of the guidance provided by the MUT inventor regarding the CI values, the location of the biopsy area indicated on the mammograms, and the histopathological reports from the biopsy of the respective lesions. This was not a blind study.

## Results

The histopathology of biopsy specimens from the 71 female volunteers with BIRADS-4 solid lesions <15 mm in maximum dimension revealed 22 cases of malignant lesions and 49 cases of high-risk or benign lesions. Invasive disease was diagnosed in 16 patients (12 ductal, one lobular, two tubular, and one mucinous carcinoma), while in situ disease was diagnosed in five patients. A cystosarcoma was diagnosed in one patient. The final pathology report, after the indicated surgical treatment, was concordant with the initial biopsy diagnosis in all patients with malignant lesions. High-risk lesions (atypical ductal hyperplasia, lobular neoplasia, and radial scar) were diagnosed in three patients, and further surgical biopsy did not reveal underestimation. The 46 patients with benign lesions (fibrocystic changes, fibroadenomas, papillomas without atypia, cysts) were followed up at a median 18 months after biopsy and did not show any mammographic signs of malignancy.

All 22 malignant lesions in this study exhibited maximum CI values greater than 1. Since the CI values are computed as the product of the respective values of refractivity and attenuation (at 2 MHz in this study), the malignant lesions corresponded to high values of *both* refractivity and attenuation, while the benign lesions exhibited high values in only one of these two attributes. This is illustrated in Figs. 1 and 3 below, where a sequence of MUT composite images (Fig. 1) as well as the corresponding refractivity and attenuation images (Fig. 3) for 15 coronal slices of volunteer #14 presenting a biopsy-confirmed malignant lesion are shown. This is the main finding of this study, and it agrees with early findings of ultrasound tomography [28–30]. The range of values for the normal breast tissues can also be seen in these figures with reference to the colour-bar scale provided at the bottom right side of each figure. Note that these values are calibrated with reference to degasified/deionized water at 30 °C, and they are demeaned when displayed as images. The statistical distributions of refractivity and attenuation values for all pixels in this set of subjects are bell-shaped and have mean (standard

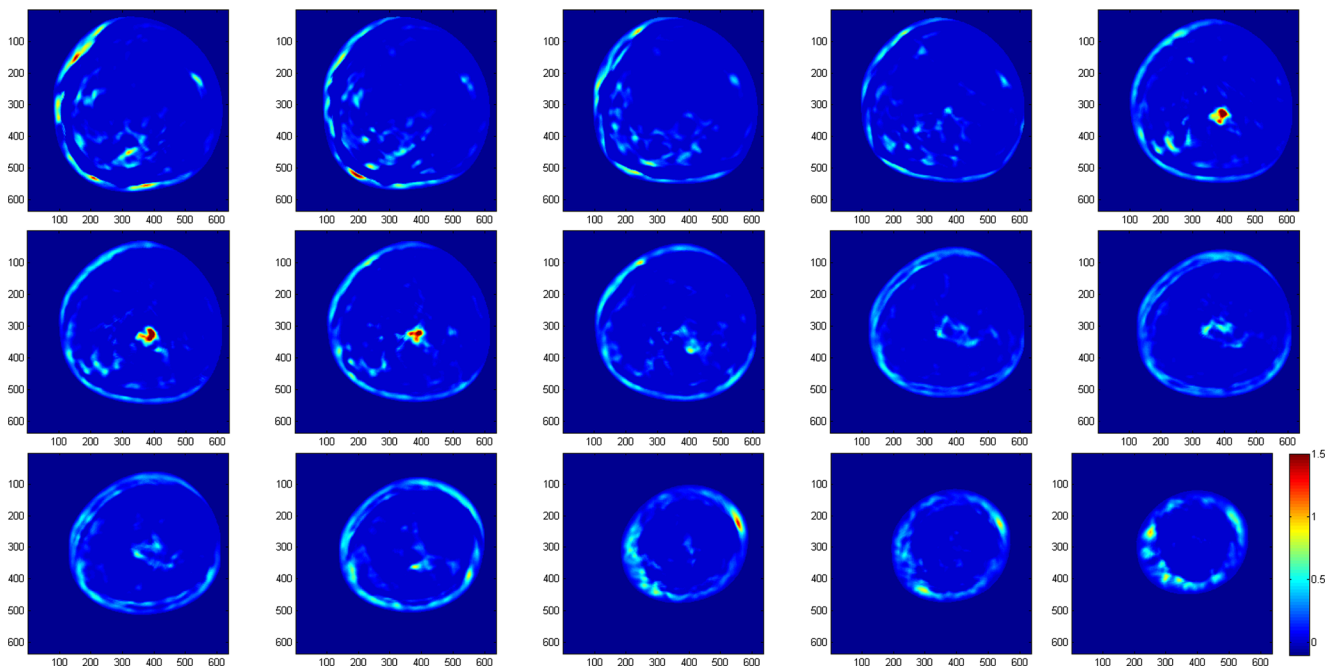


**Fig. 1** The obtained 15 successive coronal slices (4 mm apart) of MUT composite images for the left breast of volunteer #14 with a biopsy-confirmed malignant lesion (IDC), which is depicted in red near the centre of slices 5–7, because the lesion voxels have high CI values (>1). The location of the detected lesion corresponds to the biopsy

location marked with circles in the two views (CC and MLO) of the mammogram shown in Fig. 2. We note some additional red pixels in the dermal plexus region of the composite image (slices 1, 2, and 13) that are not viewed as lesions (see text)

deviation) values of -0.62 (0.57) for refractivity and 0.23 (0.68) for attenuation at 2 MHz. Due to the aforementioned definition of the CI index (i.e., the product of water-calibrated positive refractivity and attenuation values), its statistical distribution is monotonically declining and defined over positive values only. Based on the computed statistical distribution of the CI values of the pixels of all subjects in this study, 99.9 % of them were found to have CI values below 0.96. Table 1 lists the types of the 22 malignant lesions found in this set of volunteers and the corresponding averages and standard deviations (SD) of the maximum CI values that were observed for each lesion type. Note that the decision of malignancy is based on the *maximum CI value* of an apparent lesion and *not on the average CI value* over an image segment that may

correspond to an apparent lesion. For this reason, the single lesions listed in Table 1 have no SD value, and the reported “average” CI value is simply the maximum CI value in the respective single lesion.

The assessment of what constitutes a “high” value of refractivity or attenuation is based on the statistical distribution of such values for the pixels of normal breast tissue that are calibrated to a precisely controlled water-through reference (mean and SD values were given in the previous paragraph). It appears that the voxels of adipose tissue exhibit the lowest values of both attributes (refractivity and attenuation), while glandular and connective tissue exhibit intermediate values of both attributes. Cystic lesions seem to have the

**Table 1** List of averages (SD) of max CI values for biopsy-confirmed malignant lesions

Malignant Lesions	Number	Average (SD) of max Composite Index
Invasive ductal carcinoma	12	1.84 (0.33)
Ductal carcinoma in situ	5	1.23 (0.12)
Invasive lobular carcinoma	1	1.27 (N/A)
Tubular carcinoma	2	1.31 (0.08)
Invasive mucinous carcinoma	1	1.17 (N/A)
Cystosarcoma	1	1.38 (N/A)
All Malignant Lesions	22	1.57 (0.28)

distinctive characteristic of high refractivity but low attenuation, while fibrotic lesions seem to exhibit relatively high refractivity but intermediate attenuation. The voxels of fibroadenomas, papillomas, and atypical hyperplasia seem to exhibit relatively high attenuation and intermediate refractivity, leading to maximum CI values in the range of 0.5–1.

Two findings deserve special consideration. First, we note that an outer “annular region” around the perimeter of the coronal slices of all breasts exhibits consistently higher values of refractivity and attenuation. This is probably due to the increased collagen and fibronectin in the dermis, the superficial layer of thoracic fascia and Cooper’s ligaments that form an “acoustically harder” extracellular matrix in this region. For this reason, this annular region of the dermal plexus should be analysed separately (i.e., with different statistics for the CI values) from the main “stromal region” of the breast. This separate statistical analysis also applies to the coronal slices near the nipple-areolar complex, where the presence of lactiferous sinuses and the increased ratio of connective to adipose tissue cause a rise in the values of attenuation and refractivity.

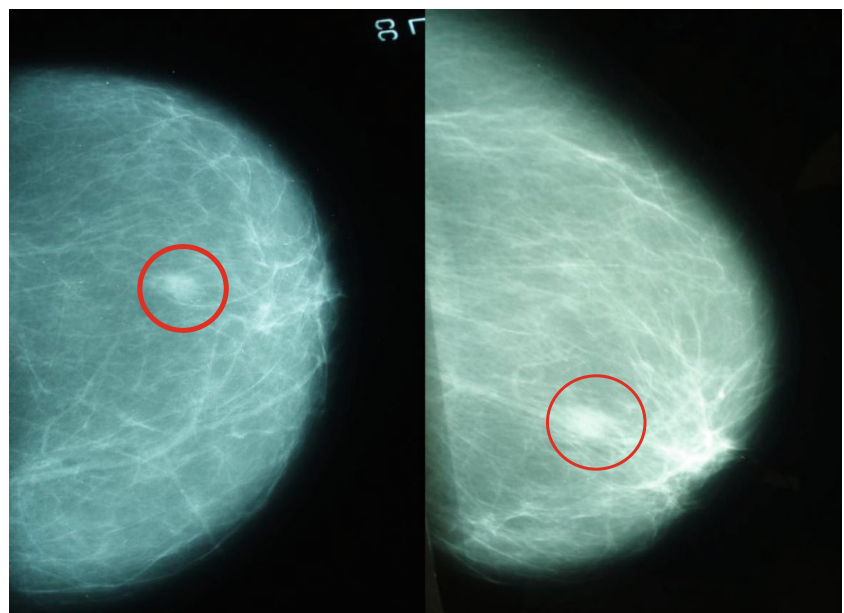
Second, there were occasional CI values above 1 that did not correspond to malignant lesions, either in the region of biopsy or elsewhere in the breast volume. This was usually (but not always) consistent with the aforementioned statistics of the distribution of the CI values for the pixels of normal tissues and benign lesions (i.e., less than 100 pixels with  $CI > 1$  in composite images of 100,000 pixels). This issue deserves further careful study, as it impacts the critical aspect of MUT specificity (see “Discussion”).

To illustrate these findings, we show in Fig. 1 the MUT composite images for 15 consecutive coronal slices (4 mm apart) of volunteer #14 with a biopsy-confirmed malignant lesion (invasive ductal carcinoma) of maximum dimension 12 mm, presented as a nodule in her mammogram shown in Fig. 2 (CC and MLO views). The dimensions of these images are 150 mm × 150 mm, with pixel size of 0.25 mm × 0.25 mm (600 × 600 pixels). The biopsy-confirmed malignant lesion is depicted in red surrounded by yellow, near the centre of the composite images for slices 5–7 (the numbering of the slices is from left to right and top-down), because the lesion voxels have high CI values ( $>1$ ) relative to the rest of the stromal breast region. The maximum CI value of this lesion was 2.34 on slice 6. We note some additional red pixels in the dermal plexus region of slices 1, 2, and 13 that are not viewed as lesions, because the normative range of CI values in the dermal plexus has been found to be about 30 % higher than the stromal region.

For illustrative purposes, we also show in Fig. 3 the sets of component images of refractivity and attenuation at 2 MHz. It is evident that these component images contain distinct types of information supporting the view of multimodal diagnostic imaging via combination of distinct acoustic attributes. Indications of the confirmed lesion exist in both sets of component images near the centre of slices 5–7 (i.e., elevated values of refractivity and attenuation). The location of the MUT-detected malignant lesion corresponds to the biopsy area marked with red circles in the two views of the mammogram shown in Fig. 2.

In order to illustrate a case with a benign lesion, in Fig. 4 we show 10 successive coronal slices for volunteer #19 presenting a biopsy-confirmed intraductal

**Fig. 2** The two views (left: CC; right: MLO) of the left breast mammogram of volunteer #14 showing a nodule near the coronal centre about 3 cm from the nipple, marked with red circles



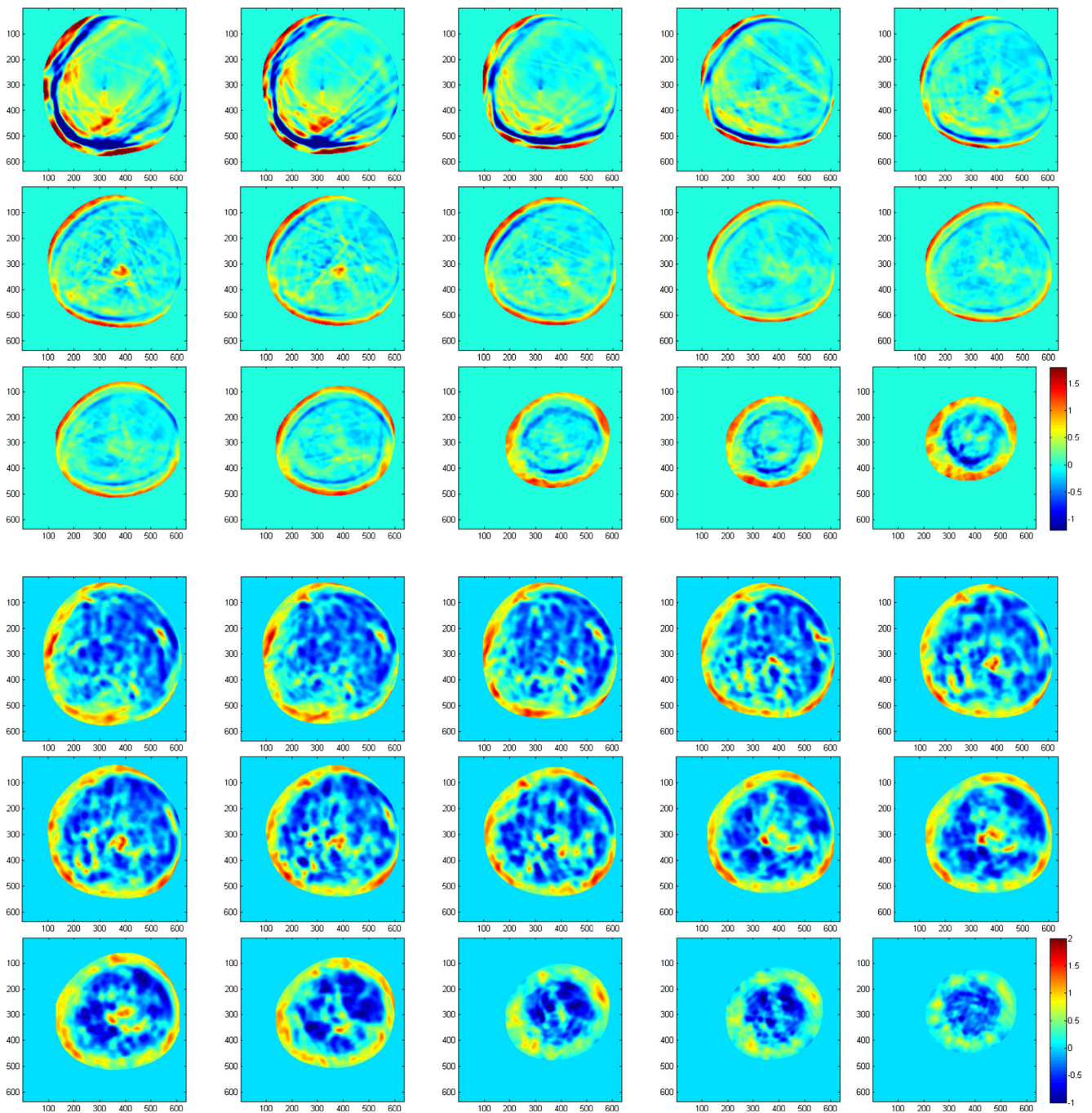


**Fig. 3** The obtained sets of 15 successive coronal slices (4 mm apart) of MUT component images of refractivity (top) and attenuation at 2 MHz (bottom) for the left breast of volunteer #14 with a biopsy-confirmed malignant lesion near the centre of slices 5–7 (see also Fig. 1). It is evident

that the two sets of component images contain distinct types of information indicative of the confirmed lesion near the centre of slices 5–7 (i.e., elevated values of refractivity and attenuation)

papilloma at approximately 6 o'clock on slices 5–6. The location of this lesion agrees with the biopsy location marked with red circles in the two views of the mammogram shown in Fig. 5. The composite index values of the pixels of this benign lesion are high relative to its surrounding tissue, but remain below 1 (the maximum CI value was 0.84 on slice 6). We note the

existence of red pixels (CI values above 1) at 8 o'clock on slice 3. We cannot confirm the presence or absence of a malignant lesion at that location because it is far from the area of biopsy. This exemplifies the key challenge of evaluating the occasional red pixels in the MUT composite images that are away from the area of biopsy. This issue of specificity of CI values is of

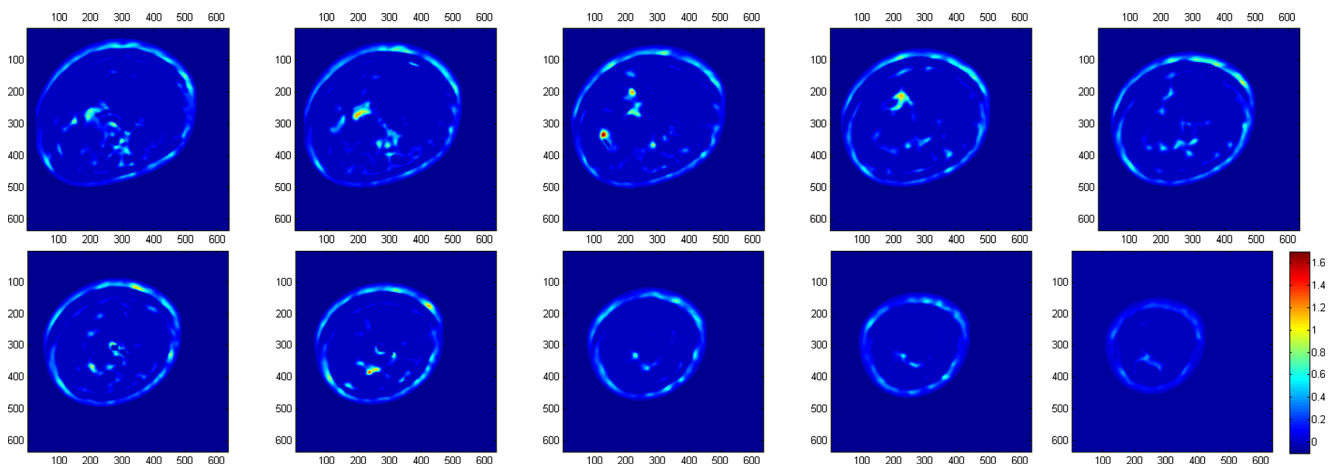


**Fig. 4** The composite MUT images for 10 successive coronal slices (4 mm apart) of the right breast of volunteer #19 presenting a biopsy-confirmed benign lesion (intraductal papilloma) at approximately 6 o'clock on slices 6–7 (shown in yellow and light blue). The location of this lesion agrees with the biopsy location marked with circles in the two

views of the mammogram shown in Fig. 5. Although the CI values of this benign lesion are high relative to the surrounding stromal tissue, they remain below 1 (the maximum CI value was 0.84 on slice 7). We note the presence of red pixels at 8 o'clock on slice 3 (see text)

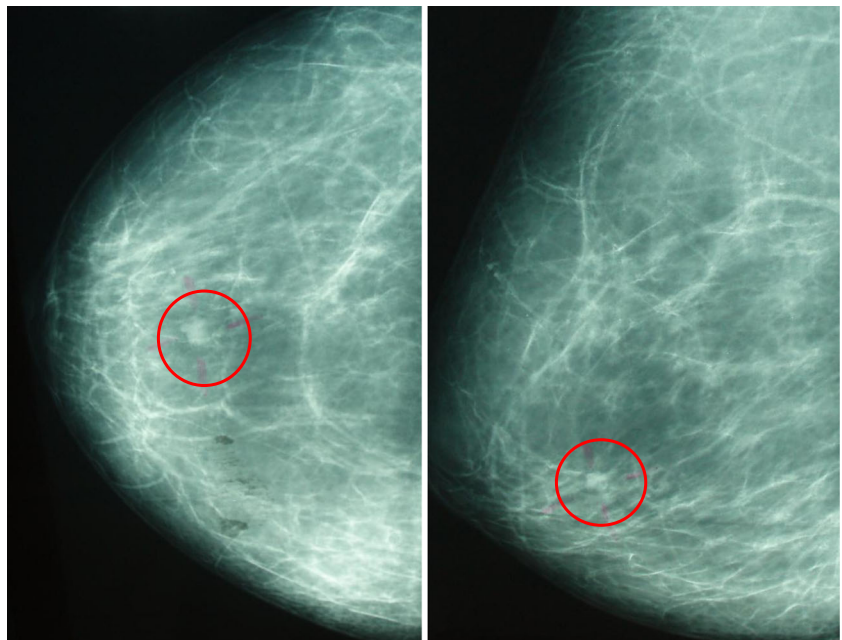
cardinal importance for future clinical applications of MUT and must be explored as a high priority in the future (see “Discussion”).

## Discussion

Using the clinical prototype of Multimodal Ultrasound Tomography (MUT) [32], we collected imaging data from 71 volunteers presenting small (<15 mm in maximum dimension) BIRADS-4 solid mammographic lesions prior to undergoing stereotactic biopsy. The histopathology reports from the biopsy and subsequent surgery, as well as 18-month follow-up

of the patients, were used to evaluate the quality of the MUT diagnostic imaging with respect to lesion detection and lesion differentiation. The results of this evaluation add to previously published results [23–27, 32] corroborating the potential utility of MUT for improved detection of small breast lesions and for reliable differentiation of malignant and benign lesions on the basis of a composite index (CI) computed from calibrated measurements of various acoustic attributes (modes) at each tissue voxel/pixel. Specifically, it was found that the maximum CI value within the pixels of each malignant lesion was above 1, corresponding to high values of *both* refractivity and attenuation. On the other hand, the maximum CI value within the pixels of each benign lesion was below 1 and exhibited

**Fig. 5** The two views (left: CC; right: MLO) of the mammogram of the right breast of volunteer #19 showing a nodule marked with red circles



high value in only one of the two attributes (refractivity and attenuation) or moderate values for both. This finding has significant diagnostic implications. The assessment of what constitutes a “high” or “moderate” value of refractivity or attenuation is based on the statistical distribution of measured values that are calibrated to precisely controlled water-through reference (see “Methods and materials”). A point of caution should be made regarding the practical difficulty of corresponding with precision the area of the biopsy to the location of the detected lesion in the MUT coronal images. Another limitation of the current MUT system is the inability to scan the axillary tail because of the positioning of the patient relative to the water bath. Our current plan to address this scanning limitation is to include in our MUT system a separate B-mode (echo-mode) module that will cover the axillary tail of the breast. Of course, this will only provide B-mode (not MUT) images for the axillary tail of the breast.

A key remaining issue is the specificity of the unique MUT lesion differentiation capability, since indications of potential additional lesions (at locations distinct from the biopsy area) were encountered in about one-third of the cases during this study. Most of these additional detections can be explained as statistical errors related to the intrinsic random fluctuations of the computed CI values (about 1 in every 1000 pixels for the current clinical prototype); however, some of these additional detections exceed these bounds of statistical error in about 15 % of the cases. Therefore, the issue must be explored with great urgency because it impacts the potential clinical utility of MUT. This will require careful, methodical, and copious study that must involve both additional medical/clinical tasks and thorough computational/statistical analysis of the values of the attributes at the lesion pixels – especially the CI values – in addition to technical improvements of the current MUT prototype that will reduce the present bounds of statistical error (1 in 1000) by a factor of about 10 – something we deem feasible in the near future. Possible strategies to meet the broader challenge of non-random additional detections include the use of follow-up MUT examinations, other sensitive imaging modalities (e.g., MRI), and detailed histopathological examination of possible mastectomy or lumpectomy specimens that may contain such suspicious MUT findings. It is evident that this issue of specificity of CI values is of cardinal importance for future clinical applications of MUT and will determine its potential as a screening modality. Therefore, this issue will be explored in the immediate future as a high-priority task.

In addition to potentially higher sensitivity and specificity than current imaging modalities, MUT offers safe and comfortable 3D imaging of the breast because it is non-ionizing and does not require breast compression or any contact. Thus, the MUT examination can be repeated safely and frequently in order to track lesion changes over time or to assess the effect of treatments. Moreover, it is operator-independent, a feature that adds to the objectivity of the measurements and may offer

significant time savings. Useful in this regard is the 3D fixed-coordinate system of MUT that allows reliable image co-registration.

If the efficacy of the MUT technology is verified, it can provide the physician with a reliable and convenient modality to assist diagnosis in the clinical context by simple inspection of the MUT composite images that can easily pinpoint the presence and 3D location of malignant lesions.

In conclusion, initial clinical results of the MUT technology seem to offer the promise of an effective diagnostic imaging modality for the detection of small breast lesions. More clinical data and careful analysis of the MUT results are required before firm conclusions can be drawn with regard to the efficacy and performance of MUT relative to current alternatives. Ongoing studies are pursuing this goal.

**Acknowledgments** The scientific guarantor of this publication is Professor George Zografos. The authors of this manuscript declare relationships with the following companies: Mastoscopia SA. The authors state that this work has not received any funding. No complex statistical methods were necessary for this paper. Approval, as required, was obtained by the Research Committee of the Hippokraton University Hospital, which acts as the institutional review board. Written informed consent was obtained from all subjects (patients) in this study. Methodology: retrospective, observational, performed at one institution.

## References

1. US Preventive Services Task Force (2009) Screening for breast cancer: U.S. preventive task force recommendation statement. *Ann Intern Med* 151:716–726
2. Gabe R, Duffy SW (2005) Evaluation of service screening mammography in practice: the impact on breast cancer mortality. *Ann Oncol* 16:153–162
3. Schopper D, de Wolf C (2009) How effective are breast cancer screening programmes by mammography? Review of the current evidence. *Eur J Cancer* 45:1916–1923
4. Baines CJ (1999) A tangled web: factors likely to affect the efficacy of screening mammography. *J Natl Cancer Inst* 91:833–838
5. Kerlikowske K, Grady D, Barclay J, Sickles EA, Ernster V (1996) Effect of age, breast density, and family history on the sensitivity of first screening mammography. *JAMA* 276:33–38
6. Helbich TH (2000) Contrast-enhanced MRI of the breast. *Eur J Radiol* 34:208–219
7. Eby PR, DeMartini WB, Peacock S, Rosen EL, Lauro B, Lehman CD (2007) Cancer yield of probably benign breast MR examinations. *J Magn Reson Imaging* 26:950–955
8. Kuhl CK, Schrading S, Leutner CC et al (2005) Mammography, breast ultrasound and MRI for surveillance of women at high familial risk for breast cancer. *J Clin Oncol* 23:8469–8476
9. Flobbe K, Bosch AM, Kessels AG et al (2003) The additional diagnostic value of ultrasonography in the diagnosis of breast cancer. *Arch Intern Med* 163:1194–1199
10. Nothacker M, Duda V, Hahn M, Warm M, Degenhardt F, Madjar H et al (2009) Early detection of breast cancer: benefits and risks of supplemental breast ultrasound in asymptomatic women with mammographically dense breast tissue. A systematic review. *BMC Cancer* 9:335–343



11. Golub RM, Parsons RE, Sigel B et al (1993) Differentiation of breast tumors by ultrasound tissue characterization. *J Ultrasound Med* 12: 601–608
12. Stavros AT, Thickman D, Rapp CL et al (1995) Solid breast nodules: use of sonography to distinguish between benign and malignant lesions. *Radiology* 196:123–134
13. Gefen S, Tretiak OJ, Piccoli CW et al (2003) ROC analysis of ultrasound tissue characterization classifiers for breast cancer diagnosis. *IEEE Trans Med Imaging* 22:170–177
14. Chen CM, Chou YH, Han KC et al (2003) Breast lesions on sonograms: computer-aided diagnosis with nearly setting independent features and artificial neural networks. *Radiology* 226:504–514
15. Smith A (2005) Full-field breast tomosynthesis. *Radiol Manag* 27: 25–31
16. Kelly KM, Dean J, Comulada WS, Lee SJ (2010) Breast cancer detection using automated whole breast ultrasound and mammography in radiographically dense breast. *Eur Radiol* 20:734–742
17. Garra BS, Cespedes EI, Ophir J, Spratt SR, Zurbier RA, Magnant CM et al (1997) Elastography of breast lesions: initial clinical results. *Radiology* 202:79–86
18. Thomas A, Fischer T, Frey H, Ohlinger R, Grunwald S, Blohmer J-U et al (2006) Real-time elastography — an advanced method of ultrasound: first results in 108 patients with breast lesions. *Ultrasound Obstet Gynecol* 28:335–340
19. Marmarelis VZ, Kim TS, Shehada REN (2003) High resolution ultrasonic transmission tomography. *Proc SPIE Med Imaging* 5035: 33–40
20. Jeong JW, Kim TS, Do SH, Shin DC, Singh M, Marmarelis VZ (2005) Soft tissue differentiation using multi-band signatures of high resolution ultrasonic transmission tomography. *IEEE Trans Med Imaging* 24:399–408
21. Marmarelis VZ, Jeong JW, Shin DC, Do SH (2007) High-resolution 3-D imaging and tissue differentiation with ultrasound transmission tomography. In: Andre ME (ed) *Acoustical imaging*, vol 28. Springer, Dordrecht, pp 195–206
22. Jeong JW, Shin DC, Do SH, Klipfel NE, Holmes DR, Hovanesian-Larsen LJ et al (2008) Differentiation of cancerous lesions in excised human breast specimens using multi-band attenuation profiles from ultrasonic transmission tomography. *J Ultrasound Med* 27:435–451
23. Zografos G, Koulocheri D, Liakou P, Sofras M, Hadjiagapis S, Orme M, Marmarelis V (2011) Detection of breast cancer via 3D multimodal ultrasound tomography. *European Congress of Radiology*, Poster No. 5349
24. Marmarelis V, Sofras M, Orme M, Hadjiagapis S, Koulocheri D, Liakou P, Zografos G (2011) Novel diagnostic imaging technology for detection of breast cancer via 3D transmission ultrasound tomography. *European Congress of Radiology*, Poster No. 5357
25. Marmarelis V, Sofras M, Orme M, Hadjiagapis S, Koulocheri D, Liakou P, Zografos (2011) Detection and differentiation of mm-size lesions in the breast using the new technology of 3D Multimodal Ultrasonic Tomography. *RSNA Conference*, Poster No. 11034449
26. Zografos G, Koulocheri D, Liakou P, Grigoropoulos P, Sofras M, Hadjiagapis S, Orme M, Forte S, Marmarelis V (2012) Non-invasive differentiation of small breast lesions via 3D MUT imaging. *European Congress of Radiology*, Paper No. B0218
27. Zografos G, Koulocheri D, Liakou P, Liouvarou I, Sofras M, Hadjiagapis S, Orme M, Marmarelis V (2014) Can transmission-ultrasound tomography detect small lesions in dense breasts? *European Congress of Radiology*, Paper No. B0465
28. Greenleaf JF, Bahn RC (1981) Clinical imaging with transmissive ultrasonic computerized tomography. *IEEE Trans Biomed Eng* 28: 177–185
29. Carson PL, Meyer CR, Scherzinger AL, Oughton TV (1981) Breast imaging in coronal planes with simultaneous pulse echo and transmission ultrasound. *Science* 214:1141–1143
30. Schreiman JS, Gisvold JJ, Greenleaf JF, Bahn RC (1984) Ultrasound transmission computed tomography of the breast. *Radiology* 150: 523–530
31. Duric N, Littrup P, Poulos L, Babkin A, Holsapple E, Rama O et al (2007) Detection of breast cancer with ultrasound tomography: first results with the computed ultrasound risk evaluation (CURE) prototype. *Med Phys* 2:773–785
32. Zografos G, Koulocheri D, Liakou P, Sofras M, Hadjiagapis S, Orme M et al (2013) Novel technology of Multimodal Ultrasound Tomography detects breast lesions. *Eur Radiol* 23:673–683